Optical Materials 115 (2021) 110994

Contents lists available at ScienceDirect

Optical Materials

journal homepage: http://www.elsevier.com/locate/optmat

Research Article

A general strategy for $CuInS_2$ based quantum dots with adjustable surface chemistry

Dominik Voigt *, Michael Bredol, Atoosa Gonabadi

FH Muenster University of Applied Sciences, Department of Chemical Engineering, Stegerwaldstr. 39, 48565, Steinfurt, Germany

ARTICLE INFO

Keywords:
Quantum dot
$CuInS_2$/ZnS
Ligand exchange
Surface modification
DFT

ABSTRACT

Different from negatively charged $CuInS_2$ (CIS) based quantum dots (QDs), positively charged QDs are difficult to obtain in good optical quality, but are desirable for certain applications. We herein present a general synthesis strategy that allows for a universal surface modification of ternary CIS based QDs with thiol containing ligands. The idea behind the synthesis design is, to apply a ZnS shell first for passivating and protecting the core QDs, and then add a second ZnS shell for the functionalization via ligand exchange. Whereby easy ligand exchange with thiolated molecules is systematically set up, by using a weak bonding amine ligand for the second shell. Molecules with various terminal groups were used to functionalize the nanoparticles and stabilize them in different media making any surface charge and polarity accessible. Surface defect chemistry seemed to play an important role in our synthesis strategy, therefore to gain a deeper understanding how these defect sites can alter the electronic structure of core/shell nanoparticles theoretical calculations based on density functional theory were performed, whilst structural, colloidal and optical properties were characterized experimentally (by dynamic light scattering, x-ray diffraction, infrared spectroscopy, zeta potential, absorption- and (time resolved) photoluminescence measurements).

1. Introduction

Quantum dots (QDs) with tunable band gaps and band edges have emerged as attractive materials for the development and enhancement of various optoelectronic materials [1]. They play an important role in the ongoing miniaturization process of nanoengineering and nanotechnology, including new catalyst materials [2–5], sensitization of solar cells [6–12], light emitting diodes [13–15], biophotonics and nanomedicine [16–19] etc. Despite II-VI and IV-VI semiconductor nanoparticles possess exceptional well-fitting optical and electronical properties, the high toxicity of the utilized heavy metal ions (Cd, Pb, Se, Te) shed doubt on their long-term applicability, especially in consideration of recent environmental regulations and restrictions. Therefore, a lot of research regarding QDs has shifted to identify and replicate such promising properties in more ecofriendly compounds. Among them ternary and quaternary semiconducting nanocrystals are presently considered as suitable alternatives to Cd and Pb chalcogenides. Ternary I-III-VI $CuInS_2$ (CIS, $E_g = 1.5$ eV) alloyed with ZnS ($E_g = 3.6$ eV) deserve here special attention, due to cost efficient production out of simple and commercially available precursors as well as precise control of their photo- and electroluminescent properties by uncomplicated modification of the preparation conditions (size, surface chemistry, composition) [20–23].

The most widely used synthesis method for high quality CIS QDs (with photoluminescence quantum yields up to 80%) consists of the reaction of the metal cation precursors (e.g. Cu(OAc) and $In(OAc)_3$) with 1-dodecanethiol (DDT) [24–26]. In this reaction DDT has the triple role of sulfur source, surface ligand and solvent and is either used alone or in a mixture with 1-octadecene (ODE). The usage of this surface ligand in the synthetic strategy is a double-edged sword, due to its strong bonding it produces very high quality nanocrystals but at the same time leads to a challenging exchangeability with other surface ligands [27]. Since DDT is hydrophobic and hasn't any functional groups, this limits the usage of the so prepared QDs due to compatibility issues. This is a potential drawback as ligand exchange is mandatory for many applications, e.g. improve the electronic coupling between nanoparticles and electrodes or substrates in solar cells [28,29] and aqueous phase transfer of the QDs for biomedical studies [30,31]. For QDs to be applicable in terms of

* Corresponding author.
E-mail address: dv009200@fh-muenster.de (D. Voigt).
URL: http://www.fh-muenster.de/ciw/personal/professoren/bredol/mitarb.php (D. Voigt).

https://doi.org/10.1016/j.optmat.2021.110994
Received 2 February 2021; Accepted 4 March 2021
Available online 11 April 2021

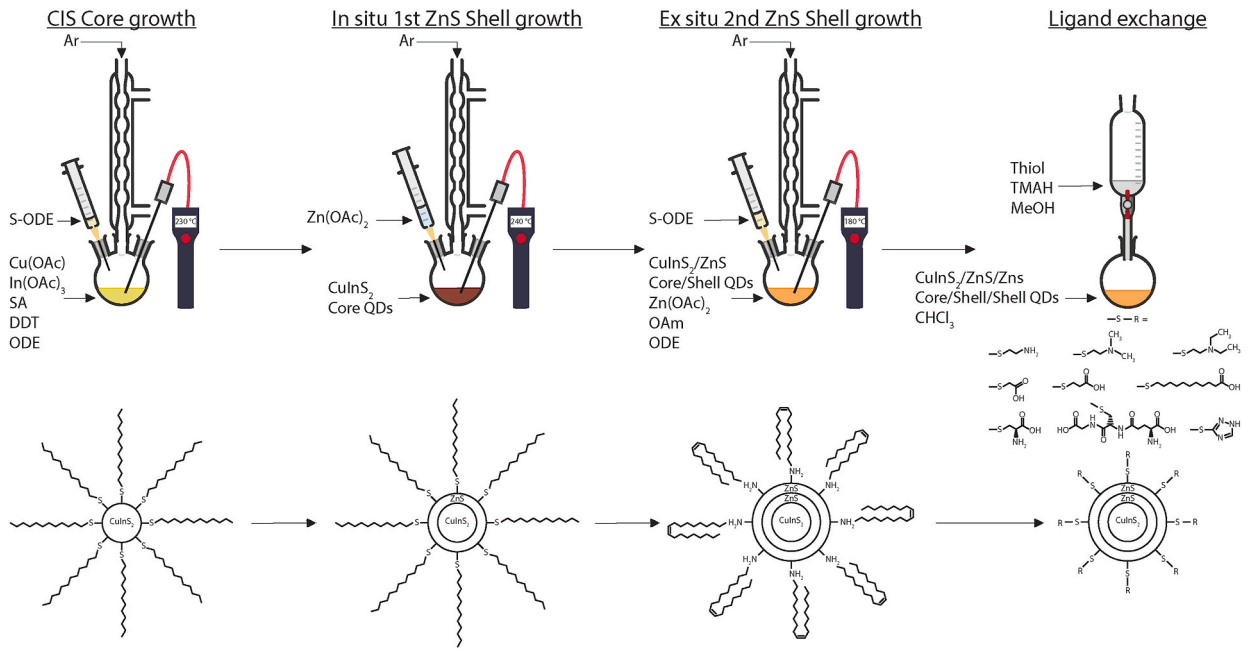

Fig. 1. Experimental scheme for the synthesis and functionalization of CIS/ZnS/ZnS.

optoelectronic purposes it is therefore necessary to manipulate the surface and interface chemistry of this material. Nevertheless, it has been shown in literature that strong bound DDT could be replaced under retaining the optical properties by 3-mercaptopropionic acid (MPA) [14, 32], 11-Mercaptoundecanoic acid (MUA) [32], 11-Mercapto-1-undecanol (MUD) [33,34] and 6-Mercaptohexanol (MCH) [35] simply by introducing these molecules into the reaction mixture after the nanocrystal growth at elevated temperatures (170 °C or higher). However, this strategy suffers from certain drawbacks, mainly that highly polar hydrophilic and temperature sensitive ligands cannot be used. Thus, e.g. there are till date only a few reports for the production of high quality CIS QDs with a positive surface charge [36].

The aim of this article is to surmount this problem and consequently obtain a broader field of application by overcoming existing compatibility issues. Thus, potentially guiding fresh experimental approaches developing new optoelectronic materials. Therefore, we introduce a two-stage shell coating of the initial nanocrystals with ZnS leading to an amine passivated outer layer while still retaining the optical properties. The amine surface ligands revealed to be easily replaceable at room temperature by a wide range of different thiols (e.g. we herein report the functionalization of high quality CIS with cysteamine as a surface ligand) leading to highly versatile functionalizable QDs. The role and influence of the ZnS shell thickness, together with surface related defects, on the optoelectronic properties was found to be of particular importance and was thus studied intensively by experimental and theoretical ab-initio methods.

2. Methods

2.1. Chemicals and reagents

Copper(I) acetate (Cu(OAc)), Indium(III) acetate ($In(OAc)_3$), Zinc acetate ($Zn(OAc)_2$), Staeric acid (SA), Sulfur (S), 1-Dodecanethiol (DDT), 1-Octadecene (ODE), Oleylamine (OAm), 2-(Dimethylamino)-ethanethiol hydrochloride (DMA), 2-(Diethylamino)-ethanethiol hydrochloride (DEA), Thioglycolic acid (TGA), 3-Mercaptopropionic acid (MPA), 11-Mercaptoundecanoic acid (MUA), L-Glutathione (L-GLU), 1H-1,2,4-Triazole-3-thiol (TAZ) and Tetramethylammonium hydroxide (TMAH) were all purchased from Sigma Aldrich. Cysteamine hydrochloride (CYS), L-Cysteine hydrochloride (L-CYS), Chloroform ($CHCl_3$), n-Hexane, Methanol (MeOH) and Toluene was obtained from Carl Roth. All reagents were used as-recieved without any prior purification step.

2.2. Synthesis of $CuInS_2$ core quantum dots

The synthetic approach was adopted from Zhang et al. [37] and modified in order to ensure thermodynamic shell growth. In a typical procedure, 73.5 mg (0.6 mmol) Cu(OAc), 175.2 mg (0.6 mmol) In $(OAc)_3$, 1023.9 mg (3.6 mmol) SA, 15.0 mL ODE and 15.0 mL DDT were loaded in a 50 mL three-neck-flask and vacuumed for 30 min at 120 °C to remove any water or oxygen that is left in the reaction mixture. Afterwards it was flushed with argon (by means of Schlenckline technology) and heated with a heating mantle under vigorous stirring to 200 °C. Then 2.4 mL of a solution prepared by dissolving 128.3 mg (4.0 mmol) of S in 10.0 mL ODE at 120 °C was injected quickly into the reaction mixture, was further heated to 230 °C and kept at that temperature for 30 min in order to allow the growth of the core CIS QDs. For the purification of the prepared core QDs the reaction mixture was cooled down to 60 °C with a water bath. Then 10 mL toluene were injected into the reaction mixture in order to stabilize the QDs. By adding MeOH the nanocrystals were precipitated and centrifuged at 10.000 rpm for 10 min. The supernatant was discarded and the underlying QDs were washed at least three more times with EtOH (T = 60 °C) to purify them.

2.3. Synthesis of $CuInS_2$/ZnS core/shell quantum dots

The growth of the first ZnS shell was carried out in situ directly after the completion of the QDs core growth. The reaction was quenched in an ice bath to temperatures of 60 °C and water free $Zn(OAc)_2$ was added as shell precursor. For details and the exact amount of $Zn(OAc)_2$ corresponding to a certain shell thickness see the supplementary information (Table S1). The mixture was heated to 240 °C and held at that temperature for 2 h to let the ZnS shell growth around the nanoparticles. The purification of these CIS/ZnS QDs is similar to that of the core CIS QDs.

2.4. Synthesis of $CuInS_2$/ZnS/ZnS core/shell/shell quantum dots

For the overgrowth of a second ZnS shell around the core/shell QDs to prepare core/shell/shell QD, 0.3 mmol of purified CIS/ZnS QDs were dissolved in 3.0 mL $CHCl_3$ and placed together with 6.0 mL OAm, 6.0

mLODE and the amount of $Zn(OAc)_2$ needed for two more ZnS monolayers (ML) in a 50 mL three-neck-flask. The flask was vacuumed at room temperature for 30 min. Afterwards it was flushed with argon and heated with a heating mantle under vigorous magnetic stirring to 180 °C. Then a stoichiometric amount of a solution prepared by dissolving 641.4 mg (20.0 mmol) of S in 20.0 mL ODE at 120 °C was injected dropwise at a rate of 0.6 mL/min into the reaction system. After the addition of the S precursor the second ZnS shell were allowed to grow for 2 h. Next the reaction mixture was cooled down to room temperature in a water bath and the CIS/ZnS/ZnS core/shell/shell QDs were precipitated by the addition of EtOH and centrifuged at 10.000 rpm for 5 min. The supernatant was discarded and the precipitate redispersed in 5.0 mL n-hexane and precipitated again by adding 10.0 mL EtOH. This washing procedure was repeated at least three times. For a simple illustration of the synthesis scheme see Fig. 1.

2.5. Ligand exchange

0.1 mmol CIS/ZnS/ZnS core/shell/shell QDs were dissolved in 5.0 mL $CHCl_3$. Under strong magnetic stirring a solution of 2.0 mmol Thiol (CYS, DMA, DEA, TGA, MPA, MUA, L-CYS, L-GLU or TAZ) and 729.2 mg (4.0 mmol) TMAH dissolved in 1.0 mL MeOH were added dropwise. Afterwards the dispersion was stirred for 2 h. The mixture was precipitated at 10.000 rpm for 10 min and washed three times with 5.0 mL bidest. H_2O and 30.0–40.0 mL Acetone. To ensure good long-term colloidal stability through a dense surface ligand coverage the precipitate was dispersed in 5.0 mL bidest. H_2O and 2.0 mmol of the corresponding thiol and refluxed for 2 h (for the MUA and TAZ samples this step was omitted, cause it led to irreversible agglomeration). The mixture was purified again as described above.

2.6. X-ray diffraction (XRD) analysis

The crystallographic structure of the prepared QDs was studied by XRD techniques using a Rigaku MiniFlex II Desktop diffractometer equipped with a radiation source from an X-Ray tube with Cu-Kα radiation ($\lambda = 1.54$ Å). Measurements were performed in a 2θ range of 20° – 80° with a scan rate of 2 °/min and 0.02° increments.

2.7. Size and zeta potential (ζ-potential) measurements

Malvern Instruments Zetasizer Nano ZS was used for particle size determination by dynamic light scattering (DLS), and zeta potential from electrophoretic mobility measurements, together with a standard pH meter (SevenMulti, Mettler Toledo). Measurements were performed from sample dispersions of 1.0 mmol/L in Water with respect to the amount of $CuInS_2$. The pH value was varied using hydrochloric acid (0.1 – 1.0 M) and sodium hydroxide (0.1 – 1.0 M). For DLS measurements a 633 nm Laser in combination with 173° backscatter detection was used. Each measurement was performed from 10 runs, each lasting 10 s. The measurements were repeated three times and the averages taken. For the zeta potential each measurement was collected from 15 runs, all experiments were repeated 3 times and the averages recorded.

2.8. Photoluminescence (PL), PL decay and absorption measurements

PL and absorption spectra as well as PL decay curves at room temperature were recorded in order to characterize the optical properties. Emission spectra were recorded using the Shimadzu Spectrofluorophotometer (RF-5301PC) equipped with a Xenon lamp (XBO 150W/CR OFR from OSRAM) with emission- and excitation monochromator slits open at a width of 3 nm. UV-VIS absorbance measurements were performed using Analytikjena Specord 200Plus. PL decay curves were measured on a fluorescence spectrometer FLS980 from Edinburg Instruments, equipped with the EPL-450 ps laser ($\lambda_{ex} = 445.6$ nm, pulse width ≤ 70 ps). For the measurements of the decay curves, the monitoring wavelength was set to the wavelength of the PL at its maximum intensity.

2.9. Fourier-transform infrared spectroscopy (FT-IR)

The adsorption of organic ligands and capping of the nanoparticles was studied by FT-IR spectroscopy using a Nicolet iS 5 with a diamond attenuated total reflectance (ATR) controller, from Thermo Fischer Scientific. Measurements were perfomed from 4000 cm^{-1} to 600 cm^{-1}.

2.10. Computational details

Calculations were performed in the framework of an ab initio density functional theory (DFT) computational method [38,39], as implemented in the Quantum ESPRESSO package [40,41]. Energies were calculated by using a plane-wave basis set, scalar relativistic ultrasoft pseudopotentials (USPP) and the generalized gradient approximation (GGA) with the Perdew-Burke-Ernzerhof (PBE) functional to describe the exchange-correlation potential [42]. To improve the accuracy of the calculations a Hubbard U correction [43] was applied on the Cu 3d In 4d Zn 3d and S 2p states to correct the well known problem that LDA and GGA functionals underestimate the band gap and aren't able to reproduce the correct position of d or f states of transition or rare earth metals [44]. Since the linear-response theory (used to calculate ab initio values for the Hubbard U parameters [45]) has its limitations and fails for closed-shell systems [46] the U parameters for Cu-d In-d Zn-d and S-p were optimized simultaneously in order to reproduce the experimental lattice parameter, band gap and the relative position of d states of ZnS and $CuInS_2$, similar to Mattioli et al. and Khan et al. [47,48]. Satisfactorily converged results were achieved by using 60 Ry as the kinetic cutoff for wavefunctions and 480 Ry as kinetic energy cutoff for the charge density and potential (see Fig. S3). The convergence thresholds for selfconsistency, the total energy, the forces for ionic minimization and the pressure for variable cell relaxations were set at 1.0×10^{-8} Ry, 1.0×10^{-4} Ry, 1.0×10^{-3} Ry/Bohr and 5.0×10^{-4} GPa respectively. A 6 × 6 × 6 Monkhorst-Pack k-point grid including the Γ point was used for sampling the 1st Brillouin zone of bulk ZnS and $CuInS_2$ while a Γ point only sampling was used for the calculation of the stand alone QDs. The supercell with the QD located at the center contains a vacuum region of at least 10 Å to avoid periodic interactions. Furthermore, to compensate surface defect states arising from dangling bonds on surface ions pseudoatoms, with fractional nuclear charges (1.75 for Cu^+, 1.25 for In^{3+}, 1.5 for Zn^{2+} and 0.5 for S^{2-}) as suggested by Huang et al. [49], were used to passivate these. Electronic band and state positions with respect to the vacuum level were obtained by calculating the planar average electrostatic potentials along the z-axis and the vacuum region is used as the absolute energy reference. The QDs were constructed by cutting out a spherical shape from the optimized underlying bulk structure by selecting all atoms within a radius of $r < x^2 + y^2 + z^2$ around a sulfur atom. All systems were optimized with respect to their geometry before any electronic structure calculation was performed.

3. Results and discussion

3.1. Synthesis and characterization of CIS/ZnS and CIS/ZnS/ZnS core/shell structures

The synthetic strategy was designed to obtain monodisperse and spherical CIS core nanoparticles. This has been realized first by balancing the reactivity of the cationic precursors (Cu^{2+}/Cu^+ being a soft Lewis acid forms stable complexes with Lewis bases like DDT and In^{3+} being a hard Lewis acid forms stable complexes with hard Lewis bases like SA), allowing for an even digestion of the Cu and In precursor and thus preventing the formation of secondary phases like Cu_xS or In_2S_3. Second, a so-called hot-injection method was used. This has the advantage over non-injection methods that nucleation and further

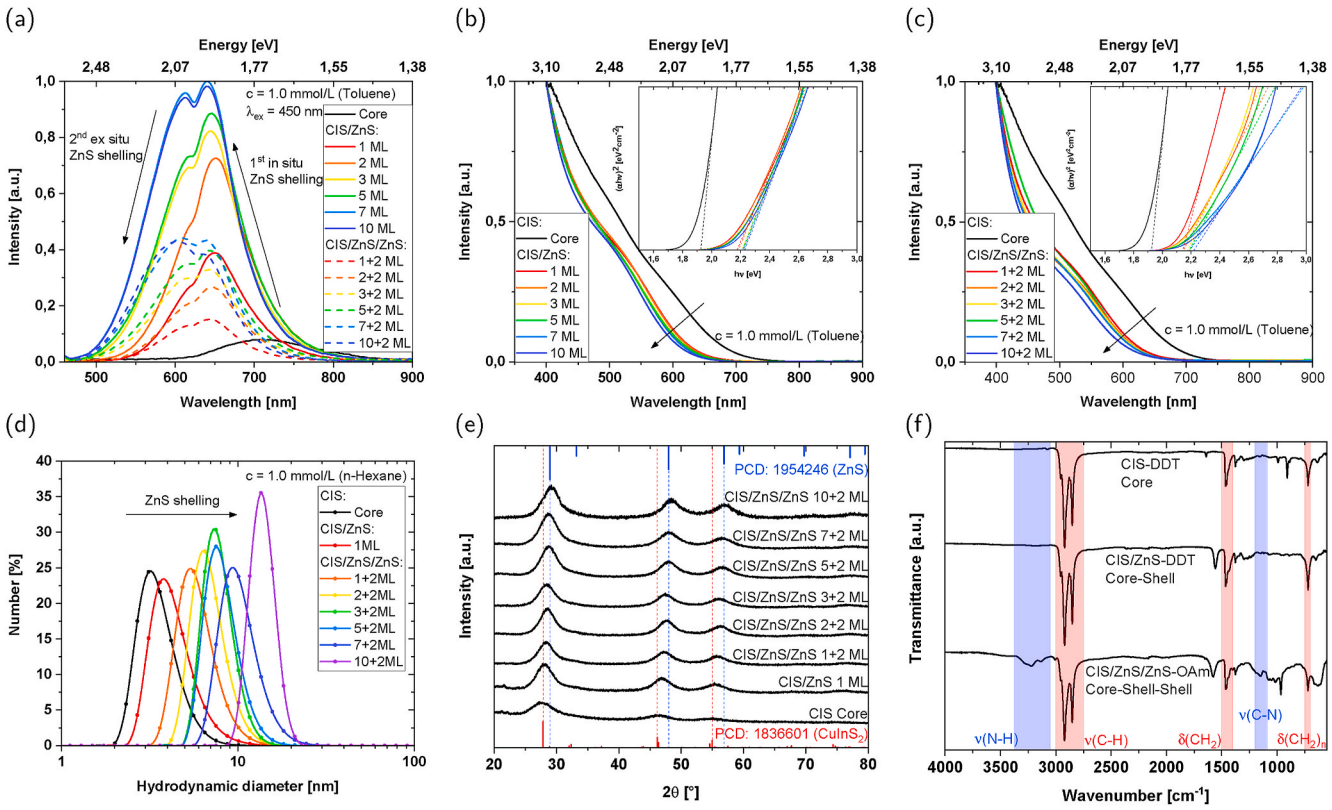

Fig. 2. PL emission spectra (a), UV-VIS absorption spectra (b,c), PSD (d), XRD pattern (e) and FT-IR spectra (f) of CIS core, CIS/ZnS core/shell and CIS/ZnS/ZnS core/shell/shell structures.

growth of the QDs occur in separate timeframes. Hot-injection leads to instantaneous nucleation and a burst of crystal seeds are produced. Because supersaturation is relieved by the nucleation burst, further growth of the nuclei into mature nanocrystals occurs via diffusion processes, such that new nucleation events do not occur and a narrow (nearly monodisperse) size distribution can be achieved [50,51]. Third, non-spherical particle shapes like cubes or tetrahedral pyramids have higher surface energies than spherical geometries, and thus requiring growth conditions characterized by a higher chemical potential [52,53]. Therefore, we improved the uniformity of spherical CIS QDs by decreasing the precursor concentration and thus also decreasing the chemical potential. Fig. S1 shows a wide field STEM image of the prepared CIS cores, confirming a narrow size distribution with an average diameter of 2.9 nm. The temporal evolution of the PL and absorption spectra (and the resulting Tauc plot) are also shown. With extending the heating time, the PL emission peak red shifts from 680 nm to 770 nm and the band gap shrinks from 2.09 eV to 1.86 eV. The reason for that is the quantum confinement effect [54], which is observed when the radius of the particle becomes smaller than the exciton Bohr radius which results in motion of the electrons and holes spatially confined to the dimension of the QD (exciton Bohr radius of CIS = 4.1 nm [55]). Analogical to the well known concept of the particle in-a-box, which increases its energy when the box size decreases, the exciton will also increase in energy. Due to the prolonged synthesis time, the CIS QDs grow and increase in size, because of diffusion processes as described above and thus the confinement energy of photogenerated electrons and holes decreases. To improve the PL efficiency, stability and resistivity of the QDs the surface is often passivated using a suitable inorganic material. For many interesting and promising semiconductor materials that crystallize in the zinc blende structure like ZnTe and InP or a derivate of it like $CuInS_2$, ZnS seems to be a near ideal candidate for forming such protective layers. That is because under ambient conditions ZnS is nontoxic, chemically stable and resistant to most environmental influences. It has a wider band gap (E_g = 3.6 eV [56]) with the conduction band minimum (CBM) and valence band maximum (VBM) being higher and lower on a total energy scale, thus creating a type-I band alignment resulting in charge carriers mainly confined to the core region. Also, the lattice mismatch is relatively low, allowing for the formation of a low-defect interface between the materials. The narrow size distribution and spherical geometry of the core material was necessary to design a shelling procedure that allows for the production of CIS/ZnS core/shell particles with a selectable amount of monolayers (ML) of ZnS. Based on the average diameter of 2.9 nm for the cores and one ML of ZnS having a thickness of 0.31 nm [57], it was possible to calculate the amount of shell precursor needed for a particular shell thickness reached from geometrical considerations (see the supplementary information for detailed information). First, CIS/ZnS core/shell structures were constructed in situ. Due to the large excess of sulfur precursor in the form of DDT no additional sulfur source needed to be injected. The zinc precursor ($Zn(OAc)_2$) was introduced at low temperatures to the CIS core mixture and then slowly heated up to avoid the formation of separate ZnS nanoparticles and to allow for even thermodynamic shell growth [58]. Since the goal of this work was the versatile surface engineering of these nanoparticles, the above already mentioned poor exchangeability of the surface ligand DDT with other surface ligands had to be overcome. Therefore, the CIS/ZnS QDs were purified till no free DDT was left in the product and then in a second ex situ approach two more ML of ZnS were grown to construct CIS/ZnS/ZnS core/shell/shell structures. In that step the stabilizing ligand was OAm, which is a strong Lewis base (forming weak bonds with Zn^{2+}, which is a weak Lewis acid) and therefore should be easily replaceable by weak Lewis bases like thiols.

As shown in Fig. 2 (a)-(c) growth of the first ZnS shell improved the emission properties substantially and blue shifted the broad and inconspicuous first excitonic absorption peak with the increase of ZnS ML. The increase in PL emission intensity can be explained by the efficient quenching of surface and internal trap states through the

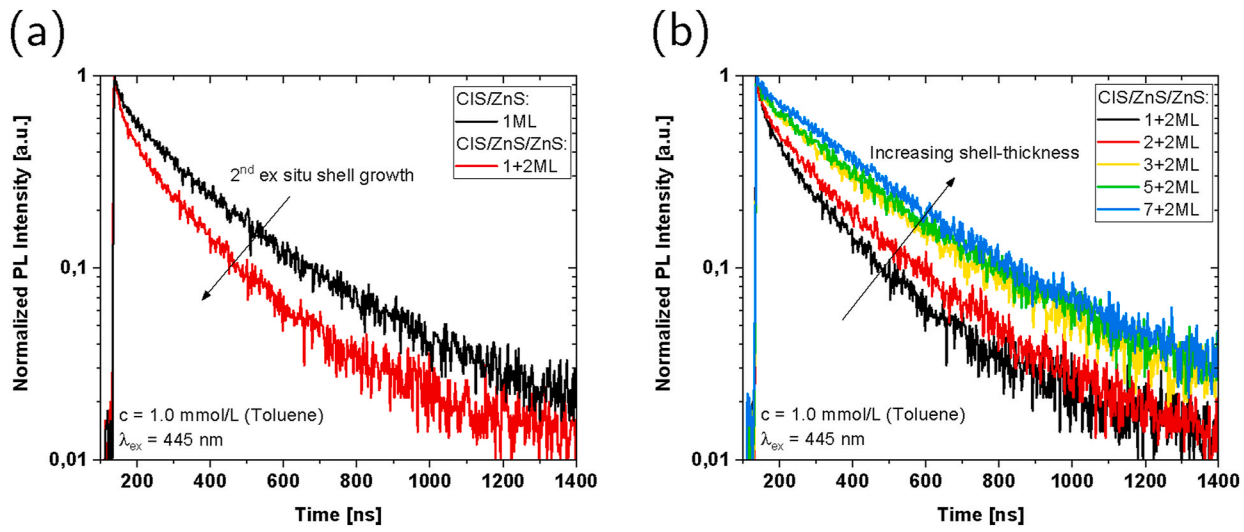

Fig. 3. PL decay curves for CIS/ZnS and CIS/ZnS/ZnS (a) and for CIS/ZnS/ZnS with different shell thicknesses (b).

Fig. 4. From left to right CIS core, CIS/ZnS with 1 ML up to 10 ML and CIS/ZnS/ZnS with 1 + 2 ML up to 10 + 2 ML under daylight and UV-light (365 nm).

Table 1
Fit parameters derived from equation (1) for PL decay curves of CIS/ZnS and CIS/ZnS/ZnS QDs.

	τ_1 [ns]	τ_2 [ns]	A_1 [%]	A_2 [%]
1 ML	42.0	296.2	36.2	63.8
1 + 2 ML	27.9	226.2	50.1	49.9
2 + 2 ML	32.8	255.2	36.3	63.7
3 + 2 ML	24.7	298.3	23.4	76.6
5 + 2 ML	26.4	314.1	21.7	78.3
7 + 2 ML	12.6	313.9	12.0	88.0

passivating layers. While the shift to higher energies (PL emission peaks (from 710 nm to 612 nm) and band gaps (from 1.93 eV to 2.23 eV)) are a result of the CIS cores shrinking [59] and the formation of ZnS alloyed CIS cores [60] through partial cation exchange combined with the saturation of surface defects. It can be seen that the second ZnS shell growth leads to decreased PL emission intensities (see also Fig. 4). Two effects might cause this: first, despite OAm being widely used in nanoparticle synthesis as solvent and ligand, it is known to be a powerful etchant in combination with elemental sulfur capable of etching sulfides, which could lead to surface etching, reconstruction and/or facetting exposing new defect sites. Yuan et al. investigated OAm-sulfur mixtures for the synthesis of chalcogenide nanostructures and found that original used seed particles dissolve in a substantial fraction only to then renucleate and regrow [61]. Second, OAm is steric more demandable than DDT, thus covering and passivating less dangling bonds of the surface atoms. Besides, it is known that such surface defects in QDs can act as charge acceptors supplying excellent channels for exciton dissociation at the QD surface [62]. With different electron-hole recombination mechanism may corresponding to different PL decay lifetimes measurements of the PL emission decay curves were performed (see Fig. 3 and Table 1) and examined. The decay curves were fitted by a biexponential function:

$$I(t) = A_1 e^{-t/\tau_1} + A_2 e^{-t/\tau_2} \quad (1)$$

where τ_1 and τ_2 represent the decay time of the PL emission and A_1 and A_2 correspond to the different decay channels relative weight.

As described in previous reports the shorter decay time (τ_1, in the order of tens of ns) can be attributed to surface- or intrinsic defect-related recombination of charge carriers whilst the longer decay time (τ_2, in the order of hundred of ns) is typical for donor-acceptor pair luminescence and therefore can be assigned to initially populated core states [59,63,64]. In Fig. 3 and Table 1 are the PL decay curves and the corresponding parameters for CIS/ZnS and CIS/ZnS/ZnS with different shell thicknesses compared. An increase in shell thickness is in general accompanied by an decrease of the first decay channel (A_1, and thus vice versa also accompanied by an increase of A_2), which can be explained by the effective reduction of surface related defects. Counterintuitively and in contrast to that the ex situ growth of the second shell, which is deposited on the nanoparticles, increases the weight of the first decay channel (A_1). These findings are in accordance with our before

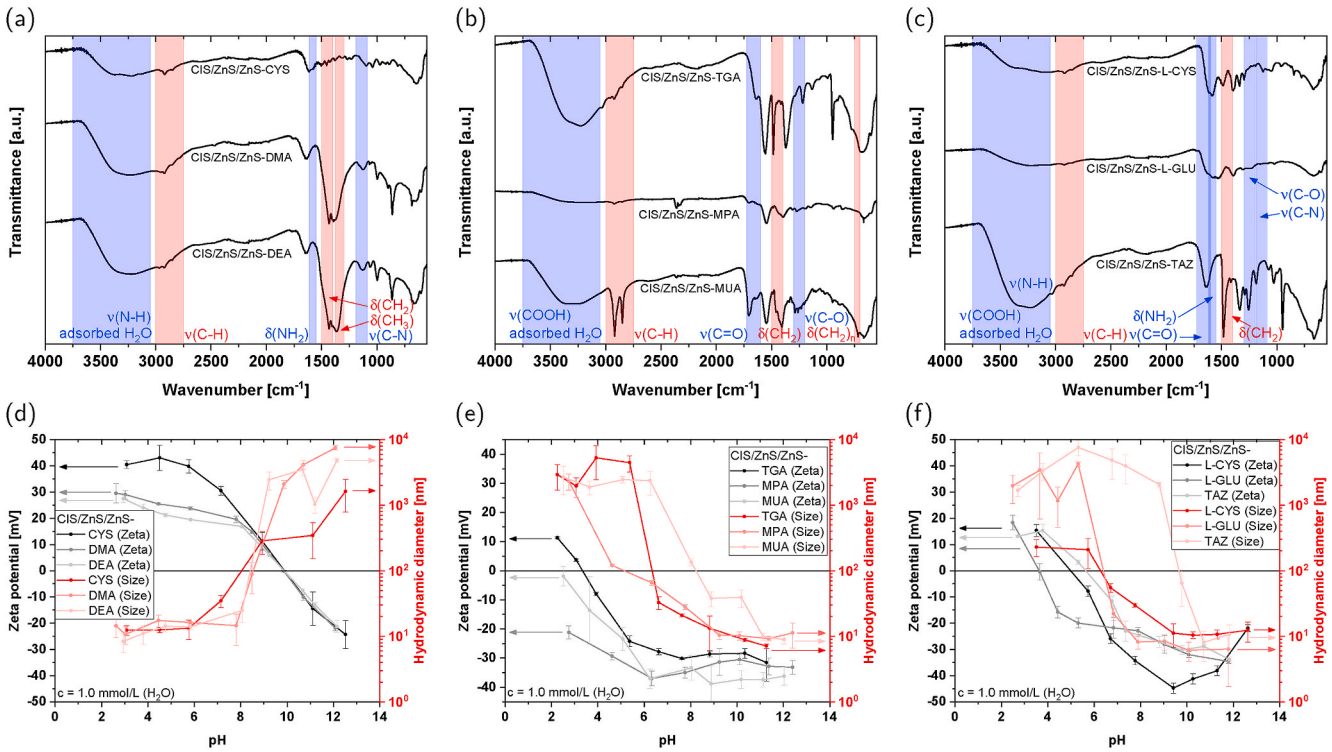

Fig. 5. FT-IR spectra of cationic (a), anionic (b), zwitterionic (c) and zeta potential and DLS size dependency of the pH value of cationic (d), anionic (e) and zwitterionic (f) functionalized CIS/ZnS/ZnS QDs.

mentioned assumption that the second ex situ shell growth leads in some degree to surface etching and reconstruction and therefore expose some new defect sites. The particle size distribution (PSD) obtained from DLS measurements is shown in Fig. 2 (d). It is noticeable that with increasing the amount of the zinc precursor the hydrodynamic diameter also increases, indicating the formation of thicker ZnS shells (larger amounts of ML). Crystal structures were examined by XRD as presented in Fig. 2 (e). The results suggest that all the samples have chalcopyrite structure and with the deposition of ZnS around the cores the diffraction peaks shift towards larger angles, consistent with the smaller lattice constant of sphalerite structure ZnS (the reference patterns are taken from the Pearson's Crystal Database (PCD)). All diffraction peaks are broadened in accordance with the finite particle size. Illustrated in Fig. 2 (f) is the FT-IR spectra of the CIS cores and the CIS/ZnS and CIS/ZnS/ZnS QDs. The distinct peaks for long chain alkyls can be observed in all samples and are attributed to DDT (in CIS core and CIS/ZnS) and OAm (in CIS/ZnS/ZnS). In consensus with our synthesis design it can be seen that after the second ex situ ZnS shell growth peaks in the region of the N–H and C–N stretching vibration appear. These belong to the OAm ligands, confirming the assumption that the surface is covered with these molecules after the second shell overcoating.

3.2. Ligand exchange

As described above, the surface engineering of the prepared CIS/ZnS/ZnS QDs that were capped with OAm should be easily achievable with the help of any thiol-containing molecules, since the affinity of Zn^{2+} is much stronger to a thiol-group than to an amine-group. In Fig. 5 (a)-(c) represented are the FT-IR spectra of cationic, anionic and zwitterionic functionalized nanoparticles, indicating with the most characteristic absorption bands (like the stretching vibration of COOH, C═O, C–O, N–H and C–N) together with adsorbed water the success of the ligand exchange. Further indication are the corresponding pH dependent zeta potential and DLS size curves in Fig. 5 (d)–(f). Functionalizing the QDs with cationic ligands like CYS, DMA and DEA led to electrostatically stabilized particles in pH regions of ∼ 2.6 – 8.1. Due to the protonation of the outward directed amine group of these ligands, the particles are charged positively at their surface in acidic conditions, repelling each other and thus leading to stable dispersions. Above that agglomeration was observed which is in agreement with increasing hydrodynamic diameters over 100 nm and decreasing zeta potentials with increasing pH values. For anionic functionalized particles with molecules like TGA, MPA and MUA its vice versa. The outward directed carboxyl group of these ligands is negatively charged due to deprotonation in basic conditions leading to stable dispersions in aqueous media in pH regions of ∼ 12.4 to 8.8. Zwitterionic ligands which possess the ability to be charged both negatively and positively should therefore be able to stabilize the QD dispersion in acidic as well as basic media. But as it is depicted in Fig. 5 (f) the particles began to agglomerate at pH values smaller than ∼ 8 and not regaining their colloidal stability at more acidic conditions. Due to low pK_a values of the acidic groups in these ligands, they are even at low pH values partly dissociated leading to overall modest zeta potentials where the charge induced repulsion between particles isn't strong enough to overcome the interatomic forces (like hydrogen bonds).

The as-prepared CIS/ZnS/ZnS QDs capped with OAm not only show good optical properties (despite being worse than the CIS/ZnS QDs capped with DDT) but they also remain highly luminescent when transferred into aqueous media. As it is shown in Fig. 6 a slight red-shift of the PL emission peak of about 10–30 nm was observed, together with variation in the magnitude of the PL peak intensity. Both effects are in accordance with literature reports and have been observed before [14, 22]. Where the emission intensity is dependent on the ligand dynamics (meaning adsorption and desorption rates of the ligands from the surface, passivating or creating surface defects) and the red-shift appeared from agglomerates of larger and smaller QDs that can then act as FRET (fluorescence resonance energy transfer) emitters.

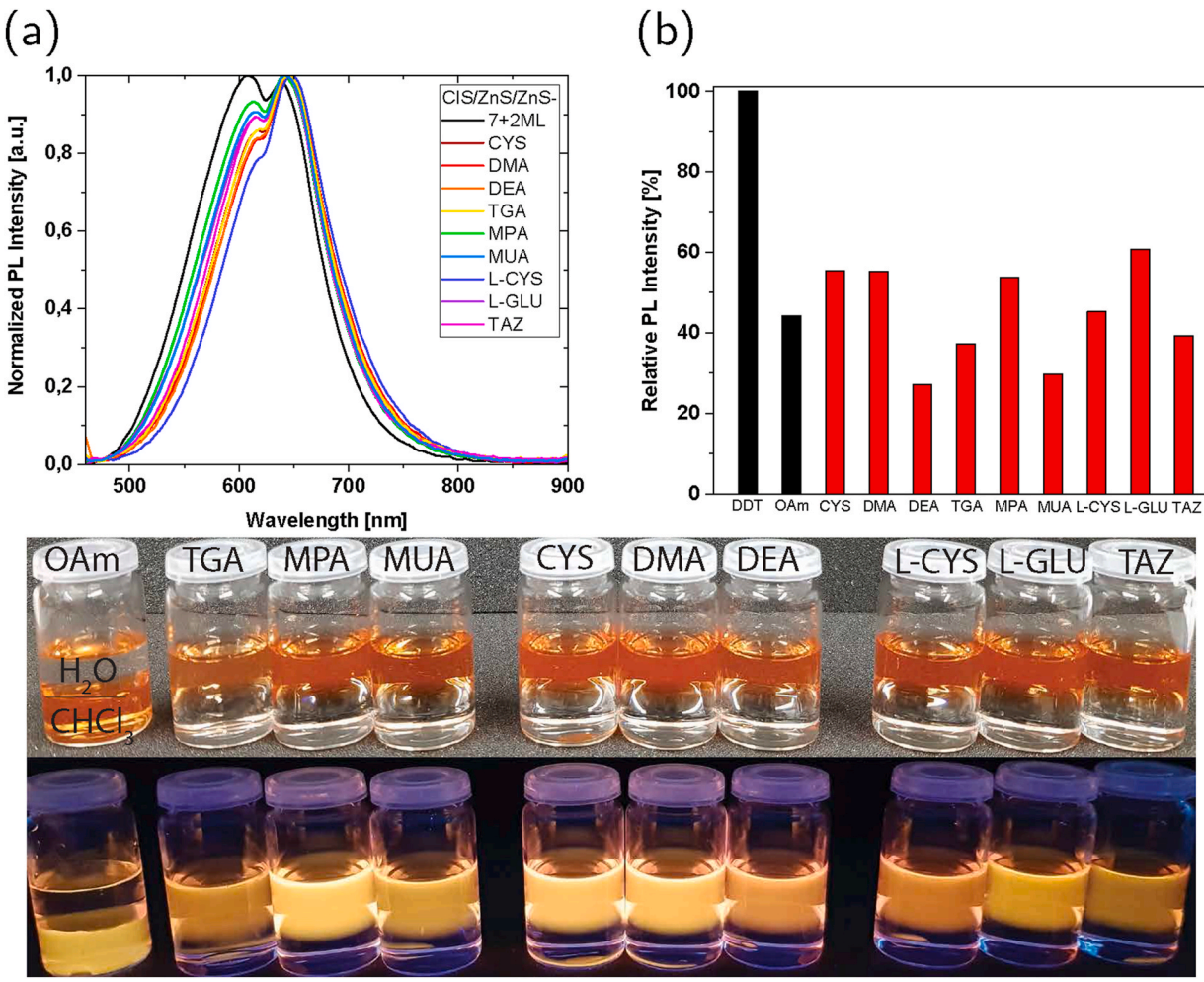

Fig. 6. PL emission spectra (a), relative PL intensity (b) and optical appearance of CIS/ZnS/ZnS QDs capped with different ligands under daylight and UV-light (365 nm).

3.3. DFT calculations

To further investigate the influence of the shelling of $CuInS_2$ with ZnS and to understand how surface defects can alter the electronic structure of core/shell nanoparticles, we performed ab initio DFT calculations. Since theoretical studies in the form of DFT calculations on quantum-confined QDs consisting of $CuInS_2$ are scarce [69] and to our best knowledge no such investigations have been performed on CIS/ZnS core/shell nanostructures, we intended to improve the accuracy of these calculations to make them as comparable to experimental results as possible. Therefore, at relatively low computational cost, the strong on-site Coulomb interaction of localized electrons which is insufficiently described by LDA or GGA is corrected by an additional Hubbard-like term (Hubbard U parameter). Analogous to our previous studies [65] the values for the U parameters were obtained semiempirically (see Fig. S4) and are 4.8 eV for S, 9.1 eV for Zn, 6.8 eV for Cu and 8.1 eV for In. The improvement from the standard GGA calculations towards more accurate results with GGA+U calculations is represented in Table S2, whereas the calculated band structure and orbital projected density of states (PDOS) for bulk sphalerite structure ZnS and chalcopyrite structure $CuInS_2$ is shown in Fig. 7. The absolute band energies are aligned with respect to the vacuum energy highlighting again that with the larger band gap of ZnS and the VBM and CBM lower and higher in energy (compared to $CuInS_2$), the formation of type-I band alignment in CIS/ZnS QDs. To validate that the before elaborated Hubbard U parameters aren't limited to bulk systems, we calculated the PDOS for different sized QDs of ZnS and $CuInS_2$, recieved their band gap and compared it to available experimental values as well as to the Brus equation (an equation based on the electronic mass approximation to calculate the band gap of semiconductor nanoparticles depending on their size [70]). The results are illustrated in Fig. 7 emphasizing once again the consequence of the quantum confinement effect (highest occupied molecular orbital (HOMO) and lowest unoccupied molecular orbital (LUMO) decreasing and increasing in energy leading to a larger band gap). To fit the size dependent trend (of our calculated results and experimental values from the literature) we use the expression:

$$E_g(d) = E_g(\infty) + \frac{1}{ad^2 + bd + c} \quad (2)$$

as proposed by Allan et al. based on tight binding calculations [71]. The R^2 and χ^2 values of these fits indicate a relatively low variance and mismatch, suggesting that the elaborated Hubbard U parameters are transferable and employable to nanosized cluster systems, also leading to meaningful results. It is also worth mentioning that the CIS cores synthesized in this work fit well into the established band gap - size dependency. In Fig. 8 the structure, PDOS, HOMO and LUMO isosurfaces (all at iso-value = 0.0001) are shown. What is immediately noticeable when the electronic structure of core/shell QDs are compared to core only QDs (same size of the core in both cases, see Fig. 7) the band gap shrinks, which is contrary to our experimental findings. This is due to some approximations in our calculational approach. First, the CIS core was completely passivated with fictional hydrogen atoms, which

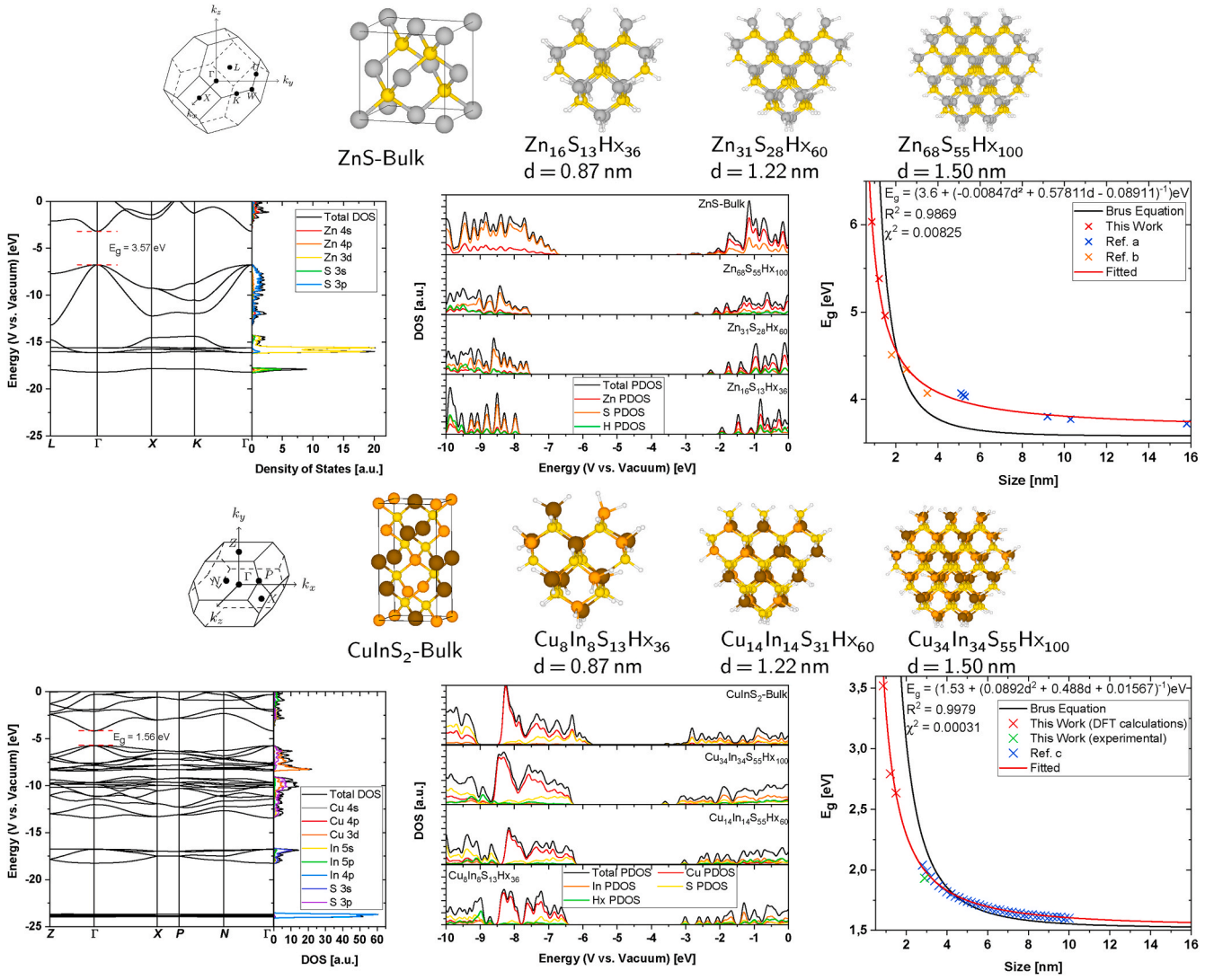

Fig. 7. 1st Brillouin zone and relaxed structures of bulk and different sized ZnS (top, reprinted from Ref. [65] under CC BY) and $CuInS_2$ (bottom) QDs (grey: Zn, yellow: S, orange: Cu, brown: In, white: Hx) and the corresponding bandstructure of the bulk material (left), the PDOS (middle), and the dependency of the QD band gap energy with respect to the particle diameter (right), Reference a [66], Reference b [67], Reference c [68].

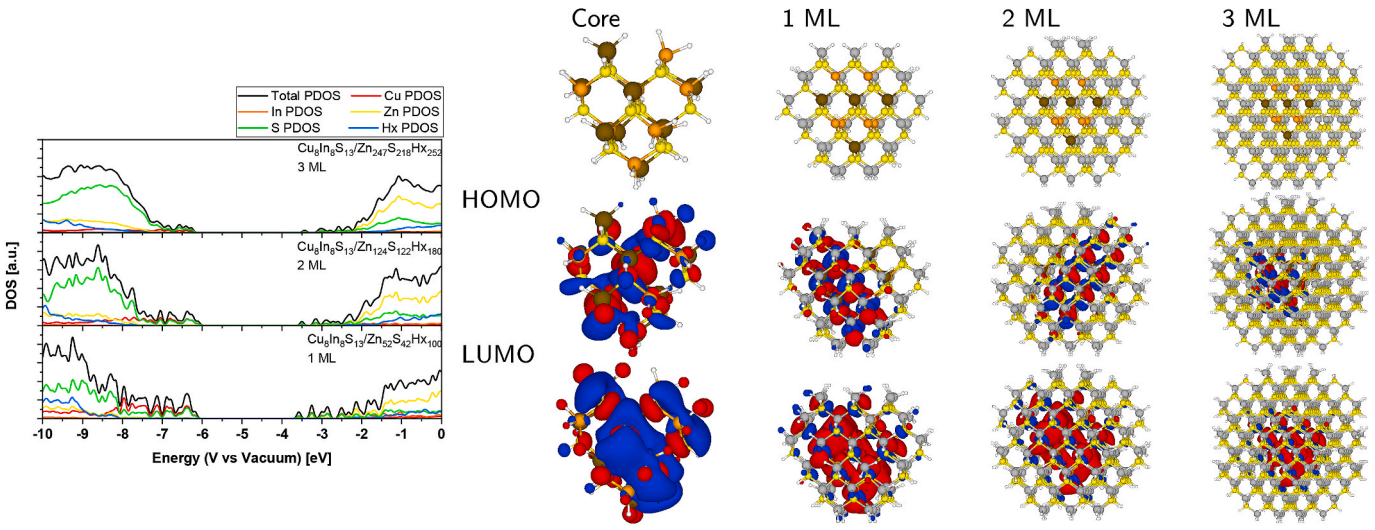

Fig. 8. PDOS of $CuInS_2$ QDs with different amounts of ML, their structure (note that the 1 ML, 2 ML and 3 ML structures are cut in half in the first row to actually see the core/shell structure) and isosurfaces of the HOMO and LUMO (red = positive, blue = negative).

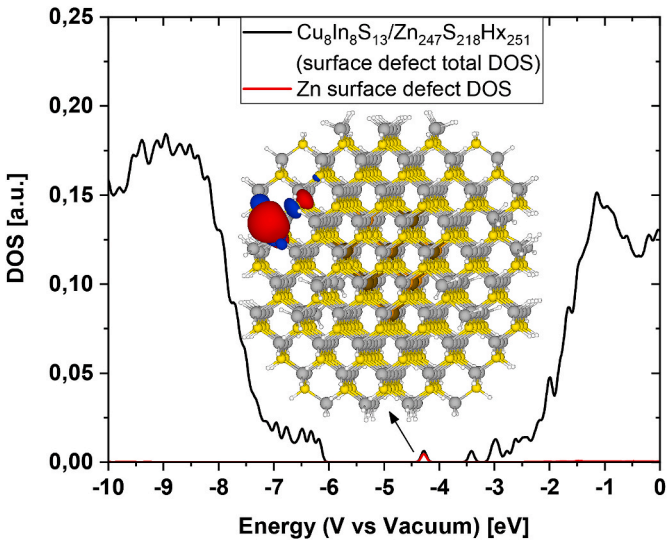

Fig. 9. PDOS of surface defect CIS/ZnS core/shell quantum dot (with 3 ML) and the defect corresponding frontier orbital of the surface.

ensures an ideal saturation of the dangling bonds suppressing all surface related defects. Second, as already described above, during the experimental shell growth the core shrinks and becomes alloyed with ZnS due to diffusion and cation exchange, which wasn't considered in our calculations. Therefore, the exchange of the near perfect passivation model in form of fictional hydrogen atoms against layers of ZnS, leads due to the lattice mismatch between $CuInS_2$ and ZnS to structural rearrangements at the interface, and thus since the energy is a function of the geometry causing the change of the electronic structure.

As it can be seen from the PDOS, increasing the number of ML increases the band gap slightly from 2.60 eV (1 ML) to 2.83 eV (3 ML), which is in agreement to the experimental observed blue shift of the band gap. Suggesting that the change in the band gap energy, when growing a passivating shell around QDs includes more factors than, as described above, passivating surface related defects, alloying the core material and shrinking the core size due to thermal diffusion and cation exchange processes. This is also reflected by the isosurfaces of the HOMO and LUMO, as the wavefunctions are stronger confined to the core region. However, it should be mentioned that in every model the wavefunction extends to a certain degree beyond the core/shell interface. To test our hypotheses, that surface defects on the passivating ZnS shell can alter the optoelectronic properties and are an explanation for the decrease in PL emission intensity after the second ex situ shell growth, we removed one of the fictional hydrogen atoms that saturate the dangling bonds of the surface atoms. The PDOS and frontier orbital of the defect state are shown in Fig. 9. Creation of surface defects on the ZnS layer gives rise to states whose energetic position is right in between the band gap. These states are close enough to the LUMO to act as electron acceptor traps, which would explain the experimentally observed decline in PL intensity. It should also be mentioned that the PL characteristics could be influenced through ligand exchange (see section 3.2 *Ligandexchange*), which further supports this assumption.

4. Conclusion

In summary, a general applicable route for the versatile surface engineering of CIS/ZnS/ZnS is demonstrated. The nanoparticles were functionalized with various cationic, anionic and zwitterionic thiolated ligands to yield stable aqueous dispersions. For e.g. we herein report the synthesis of high quality $CuInS_2$ based QDs capped with ligands like DMA, DEA and TAZ which to our best knowledge haven't been reported before. Steady-state and time-resolved photoluminescence studies together with DFT calculations reveal however that during the second shell growth the first protective layer must be attacked by the used precursors, leading to diminished PL intensities. Therefore, further studies could address this problem. Nevertheless, to universally change the surface properties of QDs as desired, is an important factor for the design of new optoelectronic materials or to overcome existing compatibility issues, so that our contribution is potentially guiding fresh experimental approaches.

Credit authorship contribution statement

Dominik Voigt: Conceptualization, methodology, writing - original draft preparation, writing - review and editing, visualization. **Michael Bredol:** Conceptualization, supervision, writing - original draft preparation, writing - review and editing, funding acquisition. **Atoosa Gonabadi:** Methodology, visualization.

Declaration of competing interest

The authors declare that they have no known competing financial interests or personal relationships that could have appeared to influence the work reported in this paper.

Acknowledgments

This research was funded in parts by the 'European Fund for Regional Development'. Computational ressources were generously provided by the 'Campus Cluster' facility from the university of applied sciences Muenster. The authors also gratefully appreciate the help of Holger Uphoff (FH Muenster University of Applied Sciences) for the STEM investigations, and Dr. David Enseling (FH Muenster University of Applied Sciences) for the instruction into measurement and evaluation of time resolved PL spectroscopy.

Appendix A. Supplementary data

Supplementary data to this article can be found online at https://doi.org/10.1016/j.optmat.2021.110994.

References

[1] D. Bera, L. Qian, T.K. Tseng, P.H. Holloway, Quantum dots and their multimodal applications: a review, Materials (Basel) 3 (2010) 2260–2345.
[2] H. Cheng, X.J. Lv, S. Cao, Z.Y. Zhao, Y. Chen, W.F. Fu, Robustly photogenerating H2 in water using FeP/CdS catalyst under solar irradiation, Sci. Rep. 6 (2016) 1–10.
[3] Y.J. Gao, X.B. Li, H.L. Wu, S.L. Meng, X.B. Fan, M.Y. Huang, Q. Guo, C.H. Tung, L. Z. Wu, Exceptional catalytic nature of quantum dots for photocatalytic hydrogen evolution without external cocatalysts, Adv. Funct. Mater. 28 (2018) 1–8.
[4] S. Yu, X.B. Fan, X. Wang, J. Li, Q. Zhang, A. Xia, S. Wei, L.Z. Wu, Y. Zhou, G. R. Patzke, Efficient photocatalytic hydrogen evolution with ligand engineered all-inorganic InP and InP/ZnS colloidal quantum dots, Nat. Commun. 9 (2018) 1–10.
[5] J. Huang, B. Xu, L. Tian, P.B. Pati, A.S. Etman, J. Sun, L. Hammarström, H. Tian, A heavy metal-free CuInS2 quantum dot sensitized NiO photocathode with a Re molecular catalyst for photoelectrochemical CO2 reduction, Chem. Commun. 55 (2019) 7918–7921.
[6] J.Y. Chang, S.C. Chang, S.H. Tzing, C.H. Li, Development of nonstoichiometric CuInS2 as a light-harvesting photoanode and catalytic photocathode in a sensitized solar cell, ACS Appl. Mater. Interfaces 6 (2014) 22272–22281.
[7] E.H. Sargent, Colloidal quantum dot solar cells, Nat. Photonics 6 (2012) 133–135.
[8] Y. Cao, A. Stavrinadis, T. Lasanta, D. So, G. Konstantatos, The role of surface passivation for efficient and photostable PbS quantum dot solar cells, Nat. Energy 1 (2016) 1–6.
[9] Y.H. Chiang, K.Y. Lin, Y.H. Chen, K. Waki, M.A. Abate, J.C. Jiang, J.Y. Chang, Aqueous solution-processed off-stoichiometric Cu-In-S QDs and their application in quantum dot-sensitized solar cells, J. Mater. Chem. A 6 (2018) 9629–9641.
[10] G. Wang, H. Wei, J. Shi, Y. Xu, H. Wu, Y. Luo, D. Li, Q. Meng, Significantly enhanced energy conversion efficiency of CuInS2quantum dot sensitized solar cells by controlling surface defects, Nano Energy 35 (2017) 17–25.
[11] J. Luo, H. Wei, Q. Huang, X. Hu, H. Zhao, R. Yu, D. Li, Y. Luo, Q. Meng, Highly efficient core-shell CuInS2-Mn doped CdS quantum dot sensitized solar cells, Chem. Commun. 49 (2013) 3881–3883.

[12] X. Zhang, X. Huang, Y. Yang, S. Wang, Y. Gong, Y. Luo, D. Li, Q. Meng, Investigation on new CuInS2/carbon composite counter electrodes for CdS/CdSe cosensitized solar cells, ACS Appl. Mater. Interfaces 5 (2013) 5954–5960.
[13] Y.H. Won, O. Cho, T. Kim, D.Y. Chung, T. Kim, H. Chung, H. Jang, J. Lee, D. Kim, E. Jang, Highly efficient and stable InP/ZnSe/ZnS quantum dot light-emitting diodes, Nature 575 (2019) 634–638.
[14] K. Gugula, L. Stegemann, P.J. Cywiński, C.A. Strassert, M. Bredol, Facile surface engineering of CuInS2/ZnS quantum dots for LED down-converters, RSC Adv. 6 (2016) 10086–10093.
[15] K. Gugula, M. Entrup, L. Stegemann, S. Seidel, R. Pöttgen, C.A. Strassert, M. Bredol, Solid solution quantum dots with tunable dual or ultrabroadband emission for LEDs, ACS Appl. Mater. Interfaces 9 (2017) 521–528.
[16] G. Xu, S. Zeng, B. Zhang, M.T. Swihart, K.T. Yong, P.N. Prasad, New generation cadmium-free quantum dots for biophotonics and nanomedicine, Chem. Rev. 116 (2016) 12234–12327.
[17] D. Deng, Y. Chen, J. Cao, J. Tian, Z. Qian, S. Achilefu, Y. Gu, High-quality CuInS 2/ZnS quantum dots for in vitro and in vivo bioimaging, Chem. Mater. 24 (2012) 3029–3037.
[18] I.A. Mir, V.S. Radhakrishanan, K. Rawat, T. Prasad, H.B. Bohidar, Bandgap tunable AgInS based quantum dots for high contrast cell imaging with enhanced photodynamic and antifungal applications, Sci. Rep. 8 (2018) 1–12.
[19] A. Arshad, R. Akram, S. Iqbal, F. Batool, B. Iqbal, B. Khalid, A.U. Khan, Aqueous synthesis of tunable fluorescent, semiconductor CuInS2 quantum dots for bioimaging, Arab. J. Chem. 12 (2019) 4840–4847.
[20] J. Zhang, R. Xie, W. Yang, A simple route for highly luminescent quaternary Cu-Zn-In-S nanocrystal emitters, Chem. Mater. 23 (2011) 3357–3361.
[21] D. Pan, D. Weng, X. Wang, Q. Xiao, W. Chen, C. Xu, Z. Yang, Y. Lu, Alloyed semiconductor nanocrystals with broad tunable band gaps, Chem. Commun. (2009) 4221–4223.
[22] G. Gabka, P. Bujak, K. Giedyk, K. Kotwica, A. Ostrowski, K. Malinowska, W. Lisowski, J.W. Sobczak, A. Pron, Ligand exchange in quaternary alloyed nanocrystals - a spectroscopic study, Phys. Chem. Chem. Phys. 16 (2014) 23082–23088.
[23] G. Gabka, P. Bujak, M. Gryszel, K. Kotwica, A. Pron, Anchor groups effect on spectroscopic and electrochemical properties of quaternary nanocrystals Cu-in-Zn-S capped with arylamine derivatives, J. Phys. Chem. C 119 (2015) 9656–9664.
[24] D. Deng, Y. Chen, J. Cao, J. Tian, Z. Qian, S. Achilefu, Y. Gu, High-quality CuInS 2/ZnS quantum dots for in vitro and in vivo bioimaging, Chem. Mater. 24 (2012) 3029–3037.
[25] S.S. Chetty, S. Praneetha, S. Basu, C. Sachidanandan, A.V. Murugan, Sustainable, rapid synthesis of bright-luminescent CuInS2-ZnS alloyed nanocrystals: multistage nano-xenotoxicity assessment and intravital fluorescence bioimaging in Zebrafish-embryos, Sci. Rep. 6 (2016) 1–15.
[26] D.E. Nam, W.S. Song, H. Yang, Facile, air-insensitive solvothermal synthesis of emission-tunable CuInS2/ZnS quantum dots with high quantum yields, J. Mater. Chem. 21 (2011) 18220–18226.
[27] M. Gromova, A. Lefrançois, L. Vaure, F. Agnese, D. Aldakov, A. Maurice, D. Djurado, C. Lebrun, A. De Geyer, T.U. Schülli, S. Pouget, P. Reiss, Growth mechanism and surface state of CuInS2 nanocrystals synthesized with dodecanethiol, J. Am. Chem. Soc. 139 (2017) 15748–15759.
[28] C.C. Chang, J.K. Chen, C.P. Chen, C.H. Yang, J.Y. Chang, Synthesis of eco-friendly CuInS2 quantum dot-sensitized solar cells by a combined ex situ/in situ growth approach, ACS Appl. Mater. Interfaces 5 (2013) 11296–11306.
[29] A. Lefrançois, B. Luszczynska, B. Pepin-Donat, C. Lombard, B. Bouthinon, J. M. Verilhac, M. Gromova, J. Faure-Vincent, S. Pouget, F. Chandezon, S. Sadki, P. Reiss, Enhanced charge separation in ternary P3HT/PCBM/CuInS2 nanocrystals hybrid solar cells, Sci. Rep. 5 (2015) 1–8.
[30] C. Zhao, Z. Bai, X. Liu, Y. Zhang, B. Zou, H. Zhong, Small GSH-capped CuInS2 quantum dots: MPA-assisted aqueous phase transfer and bioimaging applications, ACS Appl. Mater. Interfaces 7 (2015) 17623–17629.
[31] L. Li, T.J. Daou, I. Texier, T.T.K. Chi, N.Q. Liem, P. Reiss, Highly luminescent cuins 2/ZnS Core/Shell nanocrystals: cadmium-free quantum dots for in vivo imaging, Chem. Mater. 21 (2009) 2422–2429.
[32] C. Wada, Y. Iso, T. Isobe, H. Sasaki, Preparation and photoluminescence properties of yellow-emitting CuInS2/ZnS quantum dots embedded in TMAS-derived silica, RSC Adv. 7 (2017) 7936–7943.
[33] J. Choi, W. Choi, D.Y. Jeon, Ligand-exchange-ready CuInS2/ZnS quantum dots via surface-ligand composition control for film-type display devices, ACS Appl. Nano Mater. 2 (2019) 5504–5511.
[34] H. Kim, M. Suh, B.H. Kwon, D.S. Jang, S.W. Kim, D.Y. Jeon, In situ ligand exchange of thiol-capped CuInS2/ZnS quantum dots at growth stage without affecting luminescent characteristics, J. Colloid Interface Sci. 363 (2011) 703–706.
[35] Z. Bai, W. Ji, D. Han, L. Chen, B. Chen, H. Shen, B. Zou, H. Zhong, Hydroxyl-terminated CuInS2 based quantum dots: toward efficient and bright light emitting diodes, Chem. Mater. 28 (2016) 1085–1091.
[36] J. Ann Maria Xavier, G. Devatha, S. Roy, A. Rao, P.P. Pillai, Electrostatically regulated photoinduced electron transfer in "cationic" eco-friendly CuInS2/ZnS quantum dots in water, J. Mater. Chem. A 6 (2018) 22248–22255.
[37] W. Zhang, X. Zhong, Facile synthesis of ZnS-CuInS2-alloyed nanocrystals for a color-tunable fluorchrome and photocatalyst, Inorg. Chem. 50 (2011) 4065–4072.
[38] P. Hohenberg, W. Kohn, Inhomogeneous electron gas, Phys. Rev. 136 (1964) B864.
[39] W. Kohn, L.J. Sham, Self-consistent equations including exchange and correlation effects, Phys. Rev. 140 (1965) A1133.
[40] P. Giannozzi, S. Baroni, N. Bonini, M. Calandra, R. Car, C. Cavazzoni, D. Ceresoli, G.L. Chiarotti, M. Cococcioni, I. Dabo, A.D. Corso, S. de Gironcoli, S. Fabris, G. Fratesi, R. Gebauer, U. Gerstmann, C. Gougoussis, A. Kokalj, M. Lazzeri, L. Martin-Samos, N. Marzari, F. Mauri, R. Mazzarello, S. Paolini, A. Pasquarello, L. Paulatto, C. Sbraccia, S. Scandolo, G. Sclauzero, A.P. Seitsonen, A. Smogunov, P. Umari, R.M. Wentzcovitch, QUANTUM ESPRESSO: a modular and open-source software project for quantum simulations of materials, J. Phys. Condens. Matter 21 (2009) 395502.
[41] P. Giannozzi, O. Andreussi, T. Brumme, O. Bunau, M.B. Nardelli, M. Calandra, R. Car, C. Cavazzoni, D. Ceresoli, M. Cococcioni, N. Colonna, I. Carnimeo, A. D. Corso, S. de Gironcoli, P. Delugas, R.A. DiStasio, A. Ferretti, A. Floris, G. Fratesi, G. Fugallo, R. Gebauer, U. Gerstmann, F. Giustino, T. Gorni, J. Jia, M. Kawamura, H.-Y. Ko, A. Kokalj, E. Küçükbenli, M. Lazzeri, M. Marsili, N. Marzari, F. Mauri, N. L. Nguyen, H.-V. Nguyen, A. Otero-de-la Roza, L. Paulatto, S. Poncé, D. Rocca, R. Sabatini, B. Santra, M. Schlipf, A.P. Seitsonen, A. Smogunov, I. Timrov, T. Thonhauser, P. Umari, N. Vast, X. Wu, S. Baroni, Advanced capabilities for materials modelling with Quantum ESPRESSO, J. Phys. Condens. Matter 29 (2017) 465901.
[42] J.P. Perdew, K. Burke, M. Ernzerhof, Generalized gradient approximation made simple, Phys. Rev. Lett. 77 (1996) 3865–3868.
[43] M. Cococcioni, S. De Gironcoli, Linear response approach to the calculation of the effective interaction parameters in the LDA+U method, Phys. Rev. B Condens. Matter 71 (2005).
[44] S.A. Tolba, K.M. Gameel, B.A. Ali, H.A. Almossalami, N.K. Allam, The DFT+U: Approaches, Accuracy, and Applications, 2018.
[45] I. Timrov, N. Marzari, M. Cococcioni, Hubbard parameters from density-functional perturbation theory, Phys. Rev. B 98 (2018), 085127.
[46] K. Yu, E.A. Carter, Communication: comparing ab initio methods of obtaining effective U parameters for closed-shell materials, J. Chem. Phys. 140 (2014) 121105.
[47] G. Mattioli, S.B. Dkhil, M.I. Saba, G. Malloci, C. Melis, P. Alippi, F. Filippone, P. Giannozzi, A.K. Thakur, M. Gaceur, O. Margeat, A.K. Diallo, C. Videlot-Ackermann, J. Ackermann, A.A. Bonapasta, A. Mattoni, Interfacial engineering of P3HT/ZnO hybrid solar cells using phthalocyanines: a joint theoretical and experimental investigation, Adv. Energy Mater. 4 (2014) 1301694.
[48] M.S. Khan, L. Shi, B. Zou, Impact of vacancy defects on optoelectronic and magnetic properties of Mn-doped ZnSe, Comput. Mater. Sci. 174 (2020) 109493.
[49] X. Huang, E. Lindgren, J.R. Chelikowsky, Surface passivation method for semiconductor nanostructures, Phys. Rev. B Condens. Matter 71 (2005).
[50] V.K. Lamer, R.H. Dinegar, Theory, production and mechanism of formation of monodispersed hydrosols, J. Am. Chem. Soc. 72 (1950) 4847–4854.
[51] C. de Mello Donegá, P. Liljeroth, D. Vanmaekelbergh, Physicochemical evaluation of the hot-injection method, a synthesis route for monodisperse nanocrystals, Small 1 (2005) 1152–1162.
[52] H. Zhong, S.S. Lo, T. Mirkovic, Y. Li, Y. Ding, Y. Li, G.D. Scholes, Noninjection gram-scale synthesis of monodisperse pyramidal CuInS 2 nanocrystals and their size-dependent properties, ACS Nano 4 (2010) 5253–5262.
[53] Y.A. Yang, H. Wu, K.R. Williams, Y.C. Cao, Synthesis of CdSe and CdTe nanocrystals without precursor injection, Angew. Chem. Int. Ed. 44 (2005) 6712–6715.
[54] T. Takagahara, K. Takeda, Theory of the quantum confinement effect on excitons in quantum dots of indirect-gap materials, Phys. Rev. B 46 (1992) 15578–15581.
[55] J. Kolny-Olesiak, H. Weller, Synthesis and Application of Colloidal CuInS2 Semiconductor Nanocrystals, 2013.
[56] L. Ley, R.A. Pollak, F.R. McFeely, S.P. Kowalczyk, D.A. Shirley, Total valence-band densities of states of III-V and II-VI compounds from x-ray photoemission spectroscopy, Phys. Rev. B 9 (1974) 600–621.
[57] S. Taniguchi, M. Green, The synthesis of CdTe/ZnS core/shell quantum dots using molecular single-source precursors, J. Mater. Chem. C 3 (2015) 8425–8433.
[58] B. Ji, S. Koley, I. Slobodkin, S. Remennik, U. Banin, ZnSe/ZnS core/shell quantum dots with superior optical properties through thermodynamic shell growth, ACS Appl. Mater. Interfaces 22 (2020) 20.
[59] L. Li, A. Pandey, D.J. Werder, B.P. Khanal, J.M. Pietryga, V.I. Klimov, Efficient synthesis of highly luminescent copper indium sulfide-based core/shell nanocrystals with surprisingly long-lived emission, J. Am. Chem. Soc. 133 (2011) 1176–1179.
[60] J. Park, S.W. Kim, CuInS2/ZnS core/shell quantum dots by cation exchange and their blue-shifted photoluminescence, J. Mater. Chem. 21 (2011) 3745–3750.
[61] B. Yuan, X. Tian, S. Shaw, R.E. Petersen, L. Cademartiri, Sulfur in oleylamine as a powerful and versatile etchant for oxide, sulfide, and metal colloidal nanoparticles, Phys. Status Solidi 214 (2017) 1600543.
[62] M. Jones, S.S. Lo, G.D. Scholes, Quantitative modeling of the role of surface traps in CdSe/CdS/ZnS nanocrystal photoluminescence decay dynamics, Proc. Natl. Acad. Sci. U.S.A. 106 (2009) 3011–3016.
[63] J. Sun, M. Ikezawa, X. Wang, P. Jing, H. Li, J. Zhao, Y. Masumoto, Photocarrier recombination dynamics in ternary chalcogenide CuInS2 quantum dots, Phys. Chem. Chem. Phys. 17 (2015) 11981–11989.
[64] Q. Wu, C. Cai, L. Zhai, J. Wang, F. Kong, Y. Yang, L. Zhang, C. Zou, S. Huang, Zinc dopant inspired enhancement of electron injection for CuInS2 quantum dot-sensitized solar cells, RSC Adv. 7 (2017) 39443–39451.
[65] D. Voigt, L. Sarpong, M. Bredol, Tuning the optical band gap of semiconductor nanocomposites—a case study with ZnS/carbon, Materials (Basel) 13 (2020) 4162.
[66] N. Soltani, E. Saion, M. Erfani, K. Rezaee, G. Bahmanrokh, G.P. Drummen, A. Bahrami, M.Z. Hussein, Influence of the polyvinyl pyrrolidone concentration on particle size and dispersion of ZnS nanoparticles synthesized by microwave irradiation, Int. J. Mol. Sci. 13 (2012) 12412–12427.
[67] J. Nanda, S. Sapra, D.D. Sarma, N. Chandrasekharan, G. Hodes, Size-selected zinc sulfide nanocrystallites: synthesis, structure, and optical studies, Chem. Mater. 12 (2000) 1018–1024.

[68] T. Akdas, J. Walter, D. Segets, M. Distaso, B. Winter, B. Birajdar, E. Spiecker, W. Peukert, Investigation of the size-property relationship in CuInS2 quantum dots, Nanoscale 7 (2015) 18105–18118.
[69] H.D. Nelson, D.R. Gamelin, Valence-band electronic structures of Cu +-Doped ZnS, alloyed Cu- in-Zn-S, and ternary CuInS 2 nanocrystals: a unified description of photoluminescence across compositions, J. Phys. Chem. C 122 (2018) 19.
[70] L. Brus, Electronic Wave Functions in Semiconductor Clusters: Experiment and Theory, 1986.
[71] G. Allan, C. Delerue, Confinement effects in PbSe quantum wells and nanocrystals, Phys. Rev. B Condens. Matter 70 (2004) 1–9.